Ab initio determination of Kerr angles in $Cu_4Ni_8Cu_nNi_9/Cu(100)$ $(n=2-10)$

I. Reichl, R. Hammerling, A. Vernes, and P. Weinberger
Center for Computational Material Science, Vienna University of Technology, Getreidemarkt 9/134, A-1060 Vienna, Austria

C. Sommers
Laboratoire de Physique des Solides, Université de Paris-Sud 91405 Orsay Cedex, France

L. Szunyogh
Center for Computational Material Science, Vienna University of Technology, Getreidemarkt 9/134, A-1060 Vienna, Austria and Department of Theoretical Physics and Center for Applied Mathematics and Computational Physics, Budapest University of Technology and Economics, Budafoki út 8, H-1521 Budapest, Hungary
(Received 12 August 2004; published 17 December 2004)

Calculated polar magneto-optic Kerr rotation and ellipticity angles are presented for the system $Cu_4Ni_8Cu_nNi_9/Cu(100)$, $n=2,\ldots,10$. Contrary to the common belief, the Kerr signals are found to be not directly proportional to the total magnetic moment. It will be shown that in order to assign at least indirectly the size (and sign) of the Kerr angles and therefore the type of coupling to a kind of total magnetic moment, one has to consider weighted layer-resolved moments, e.g., weighted by the damping factors of the reflected waves. As to be expected the occurring oscillations in the Kerr angles with respect to the spacer thickness resemble closely those for the interlayer exchange coupling energy.

DOI: 10.1103/PhysRevB.70.214417 PACS number(s): 77.22.Ch, 78.20.Bh, 78.20.Ci, 78.20.Ls

I. INTRODUCTION

A previous article[1] reported on the experimentally recorded and theoretically calculated interlayer exchange coupling (IEC) in $Cu_4Ni_8Cu_nNi_9/Cu(100)$. It is well known that the type of coupling, antiferromagnetic (AFM) or ferromagnetic (FM), in such a multilayer system influences the shape of the hysteresis curve, a feature which is frequently exploited experimentally to record the underlying magnetic configuration. In this paper it will be shown that the type of coupling can be determined from Kerr angles θ_K and ϵ_K at vanishing external (magnetic) field, provided that for all spacer thicknesses the same (absolute) units apply for θ_K and ϵ_K.

II. THEORETICAL AND COMPUTATIONAL DETAILS

As reported in Ref. 1 all ground-state calculations were performed in using the relativistic spin-polarized screened Korringa-Kohn-Rostoker method for layered systems[2]—namely, by considering three buffer layers of Cu to guarantee reliable matching to the semi-infinite Cu(100) substrate and at least three vacuum layers to join up to the semi-infinite vacuum. All calculations of the optical conductivity tensor elements were performed fully relativistically in terms of the finite-frequency Kubo equation[3] for normal incidence of linearly polarized light with a photon wavelength corresponding to a He-Ne laser—namely, 633 nm, which is equivalent to a photon energy of 1.959 eV. All systems investigated refer exactly to those studied theoretically and experimentally in Ref. 1.

A. Substrate

In order to calculate the magneto-optic Kerr effect (MOKE) according to the 2×2 matrix technique it is necessary to know first the bulk properties of the substrate. As described in Ref. 4 the permittivity of Cu bulk was calculated by joining up two semi-infinite Cu bulk regions sandwiching $3n$ $(n=1,\ldots,6)$, monolayers (ML) of Cu. Figure 1 shows the variation of the diagonal elements $\varepsilon_{xx}=\varepsilon_{yy}$ and ε_{zz} of the permittivity tensor with the number of sandwiched Cu layers. It should be noted that only in a three-dimensional periodic (bulk) system are ε_{xx} and ε_{zz} identical, a relation that by exploiting only two-dimensional translational symmetry cannot be reproduced completely; see Ref. 4.

Figure 2 shows the differences $\mathrm{Re}(\varepsilon_{xx}-\varepsilon_{zz})$ and $\mathrm{Im}(\varepsilon_{xx}-\varepsilon_{zz})$ and a comparison of the three relative differences $|\varepsilon_{xx}-\varepsilon_{zz}|/|\varepsilon_{xx}+\varepsilon_{zz}|$, $|\varepsilon_{xx}-\varepsilon_{zz}|/(2|\varepsilon_{xx}|)$, and $|\varepsilon_{xx}-\varepsilon_{zz}|/(2|\varepsilon_{zz}|)$. As can be seen, for more than 12 sandwiched layers these

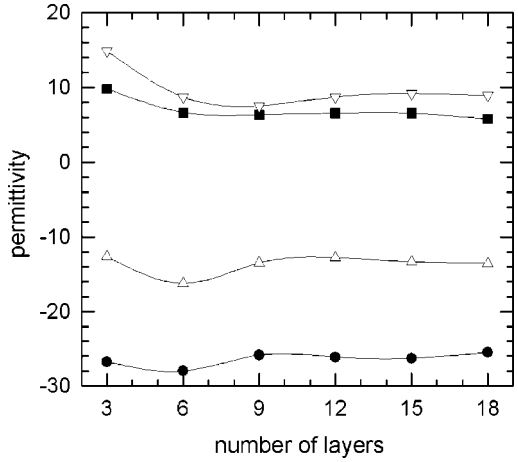

FIG. 1. Convergence of the permittivity of Cu bulk with respect to the number of sandwiched Cu layers. Circles, squares, up triangles, and down triangles denote in turn $\mathrm{Re}(\varepsilon_{xx})$, $\mathrm{Im}(\varepsilon_{xx})$, $\mathrm{Re}(\varepsilon_{zz})$, and $\mathrm{Im}(\varepsilon_{zz})$.

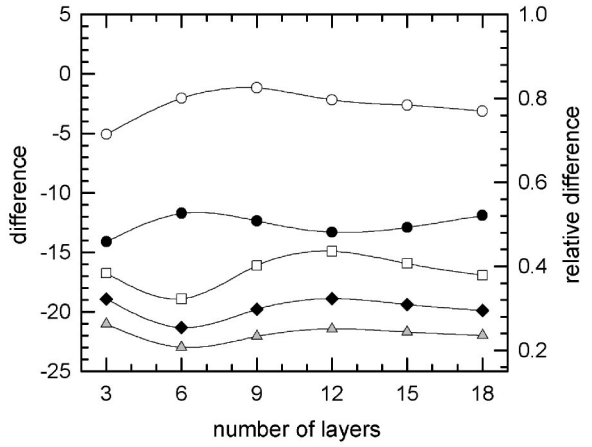

FIG. 2. The difference between the diagonal components of the permittivity of Cu bulk as a function of the number of sandwiched Cu layers. The left ordinate applies to the difference $\Delta\varepsilon \equiv \varepsilon_{xx} - \varepsilon_{zz}$ (solid circles, real part; open circles, imaginary part). The right ordinate applies to the relative differences defined as $|\Delta\varepsilon|/|\varepsilon_{xx} + \varepsilon_{zz}|$ (diamonds), $|\Delta\varepsilon|/(2|\varepsilon_{xx}|)$ (triangles), and $|\Delta\varepsilon|/(2|\varepsilon_{zz}|)$ (squares).

differences become nearly constant; i.e., the bulk value of the permittivity can be evaluated with sufficient accuracy.

B. Multilayer systems

The spacer thickness of the $Cu_4Ni_8Cu_nNi_9/Cu(100)$ system is varied between 2 and 10 ML of Cu. Since as already stated for a free surface, not only do a sufficient number of vacuum layers have to be used, but also so-called "buffer" layers to the semi-infinite substrate, and the total number of layers has to be an integral multiple of 3 (Ref. 2). Table I schematically shows the sequence of layers and the orientation of the magnetic moments for all investigated cases. In this table $\uparrow$, $\downarrow$ label the directions of the magnetization induced in the Cu layers, $\Uparrow$, $\Downarrow$ in the Ni layers, and $\times$ indicates vacuum layers in the actually investigated systems $Vac_mCu_4Ni_8Cu_nNi_9Cu_3/Cu(100)$, $m \geqslant 3$ and $2 \leqslant n \leqslant 10$. For $n=10$ both configurations—the ferromagnetic and antiferromagnetic ones—are listed since this particular case will serve later on for a comparison of their magneto-optical properties. It should be mentioned that the magnetic configuration (orientation of the moments) resulted from the IEC calculations in Ref. 1. As was shown there, the out-of-plane orientation of the moments in the Ni layers is a consequence of the lattice relaxation. Assuming that there is no distortion of the interlayer distance in the Ni slabs as compared to fcc Cu, an in-plane orientation would be preferred. At present, however, this kind of layer relaxation cannot be taken into account in the conductivity calculations. The lattice spacing considered refers to a perfect fcc Cu bulk. In all conductivity calculations the orientation of the magnetization is assumed to be out of plane (z direction).

TABLE I. Magnetic configurations (see Sec. II B).

	Number of spacer layers									
	2	3	4	5	6	7	8	9	10	
39									$\times$	
38									$\times$	
37									$\times$	Vac
36						$\times$	$\times$	$\times$	$\times$	
35						$\times$	$\times$	$\times$	$\times$	
34						$\times$	$\times$	$\times$	$\downarrow\uparrow$	
33			$\times$	$\times$	$\times$	$\times$	$\times$	$\uparrow$	$\downarrow\uparrow$	Cu_4
32			$\times$	$\times$	$\times$	$\times$	$\downarrow$	$\uparrow$	$\downarrow\uparrow$	
31			$\times$	$\times$	$\times$	$\uparrow$	$\downarrow$	$\uparrow$	$\downarrow\uparrow$	
30	$\times$	$\times$	$\times$	$\times$	$\uparrow$	$\uparrow$	$\downarrow$	$\uparrow$	$\Downarrow\Uparrow$	
29	$\times$	$\times$	$\times$	$\downarrow$	$\uparrow$	$\uparrow$	$\downarrow$	$\Uparrow$	$\Downarrow\Uparrow$	
28	$\times$	$\times$	$\uparrow$	$\downarrow$	$\uparrow$	$\uparrow$	$\Downarrow$	$\Uparrow$	$\Downarrow\Uparrow$	
27	$\times$	$\downarrow$	$\uparrow$	$\downarrow$	$\uparrow$	$\Uparrow$	$\Downarrow$	$\Uparrow$	$\Downarrow\Uparrow$	Ni_8
26	$\uparrow$	$\downarrow$	$\uparrow$	$\downarrow$	$\Uparrow$	$\Uparrow$	$\Downarrow$	$\Uparrow$	$\Downarrow\Uparrow$	
25	$\uparrow$	$\downarrow$	$\uparrow$	$\Downarrow$	$\Uparrow$	$\Uparrow$	$\Downarrow$	$\Uparrow$	$\Downarrow\Uparrow$	
24	$\uparrow$	$\downarrow$	$\Uparrow$	$\Downarrow$	$\Uparrow$	$\Uparrow$	$\Downarrow$	$\Uparrow$	$\Downarrow\Uparrow$	
23	$\uparrow$	$\Downarrow$	$\Uparrow$	$\Downarrow$	$\Uparrow$	$\Uparrow$	$\Downarrow$	$\Uparrow$	$\Downarrow\Uparrow$	
22	$\Uparrow$	$\Downarrow$	$\Uparrow$	$\Downarrow$	$\Uparrow$	$\Uparrow$	$\Downarrow$	$\Uparrow$	$\downarrow\uparrow$	
21	$\Uparrow$	$\Downarrow$	$\Uparrow$	$\Downarrow$	$\Uparrow$	$\Uparrow$	$\Downarrow$	$\uparrow$	$\downarrow\uparrow$	
20	$\Uparrow$	$\Downarrow$	$\Uparrow$	$\Downarrow$	$\Uparrow$	$\Uparrow$	$\downarrow$	$\uparrow$	$\downarrow\uparrow$	
19	$\Uparrow$	$\Downarrow$	$\Uparrow$	$\Downarrow$	$\Uparrow$	$\uparrow$	$\downarrow$	$\uparrow$	$\downarrow\uparrow$	
18	$\Uparrow$	$\Downarrow$	$\Uparrow$	$\Downarrow$	$\uparrow$	$\uparrow$	$\downarrow$	$\uparrow$	$\downarrow\uparrow$	
17	$\Uparrow$	$\Downarrow$	$\Uparrow$	$\downarrow$	$\uparrow$	$\uparrow$	$\downarrow$	$\uparrow$	$\uparrow$	Cu_n
16	$\Uparrow$	$\Downarrow$	$\uparrow$	$\downarrow$	$\uparrow$	$\uparrow$	$\uparrow$	$\uparrow$	$\uparrow$	
15	$\Uparrow$	$\downarrow$	$\uparrow$	$\downarrow$	$\uparrow$	$\uparrow$	$\uparrow$	$\uparrow$	$\uparrow$	
14	$\uparrow$	$\uparrow$	$\uparrow$	$\uparrow$	$\uparrow$	$\uparrow$	$\uparrow$	$\uparrow$	$\uparrow$	
13	$\uparrow$	$\uparrow$	$\uparrow$	$\uparrow$	$\uparrow$	$\uparrow$	$\uparrow$	$\uparrow$	$\uparrow$	
12	$\Uparrow$	$\Uparrow$	$\Uparrow$	$\Uparrow$	$\Uparrow$	$\Uparrow$	$\Uparrow$	$\Uparrow$	$\Uparrow$	
⋮	$\Uparrow$	$\Uparrow$	$\Uparrow$	$\Uparrow$	$\Uparrow$	$\Uparrow$	$\Uparrow$	$\Uparrow$	$\Uparrow$	Ni_9
4	$\Uparrow$	$\Uparrow$	$\Uparrow$	$\Uparrow$	$\Uparrow$	$\Uparrow$	$\Uparrow$	$\Uparrow$	$\Uparrow$	
3	$\uparrow$	$\uparrow$	$\uparrow$	$\uparrow$	$\uparrow$	$\uparrow$	$\uparrow$	$\uparrow$	$\uparrow$	
2	$\uparrow$	$\uparrow$	$\uparrow$	$\uparrow$	$\uparrow$	$\uparrow$	$\uparrow$	$\uparrow$	$\uparrow$	Cu_3
1	$\uparrow$	$\uparrow$	$\uparrow$	$\uparrow$	$\uparrow$	$\uparrow$	$\uparrow$	$\uparrow$	$\uparrow$	
⋮	Cu bulk									

III. RESULTS AND DISCUSSION

In Fig. 3 a comparison between the calculated IEC of Ref. 1 and the calculated Kerr angles is displayed versus the number of spacer layers (ML). It should be pointed out that the physical origin of the IEC and that of the MOKE are different and cannot be related directly. The stronger damped oscillations of the IEC values are thus not in contradiction with the moderate damping of the MOKE data. As can be seen the agreement of the oscillation periods between the MOKE results and the IEC calculations is perfect. At a first glance this seems to confirm the rule of thumb that the Kerr effect is proportional to the total magnetic moment (see Ref. 5), since in a FM configuration the total magnetic moment has to be larger than in an AFM configuration.

It should be recalled, however, that in principle the total moment is defined as the sum over all layer-resolved magnetic moments including of course not only the Ni moments

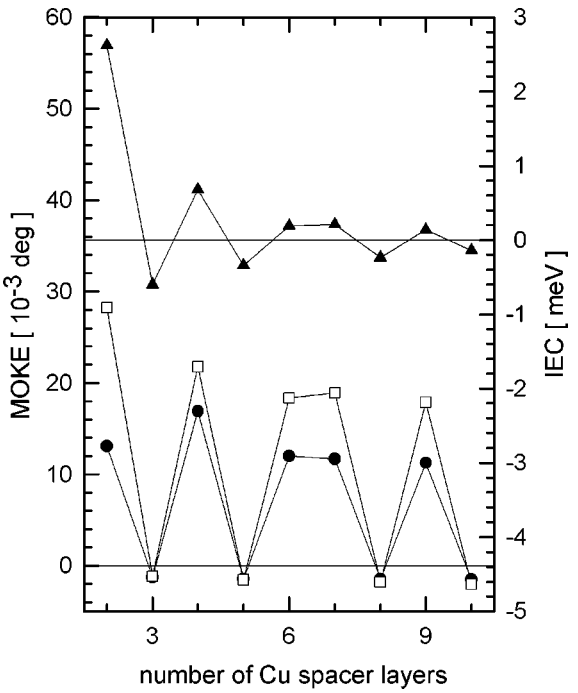

FIG. 3. Comparison between IEC and MOKE for $Cu_4Ni_8Cu_nNi_9/Cu(100)$ with respect to the number of Cu spacer layers. Triangles denote the theoretical IEC results of Ref. 1, circles and squares the calculated Kerr angles θ_K and ε_K, respectively.

but also the very weak moments in the spacer and buffer layers,

$$m = \sum_{p=1}^{N} m_p, \tag{1}$$

where N is the total number of layers considered. Clearly enough m does not change sign (z being the quantization axis) as suggested by the variation of the MOKE data with respect to the number of spacer layers (see Fig. 3), simply because 8 Ni layers always contribute less than 9 Ni layers and the Cu layers contribute very little. This in turn implies to consider first the magneto-optical properties of $Cu_4Ni_8Cu_nNi_9/Cu(100)$ before returning to the question of a possible relation to magnetic moments.

In order to sort out the difference between a FM and an AFM configuration one particular case—namely, for ten spacer layers—was considered. As can be seen from Figs. 4–7 the layer-resolved diagonal elements $\varepsilon^p_{xx}=\varepsilon^p_{yy}$ and ε^p_{zz}, do not show any peculiar differences between the two types of magnetic configurations, whereas obviously the layer-resolved off-diagonal elements ε^p_{xy} in Figs. 8 and 9 are of opposite signs in the oppositely polarized Ni slabs. It is interesting to note that essentially the paramagnetic Cu spacer layers become polarized. Polarization means that the complex off-diagonal permittivity tensor elements $\varepsilon^p_{yx}=-\varepsilon^p_{xy}$, shown in Figs. 8 and 9, do not vanish in the Cu spacer layers.

The layer-resolved permittivities ε^p_{ij}, $i,j \in \{x,y,z\}$, are the only input needed in order to calculate the Kerr angles and

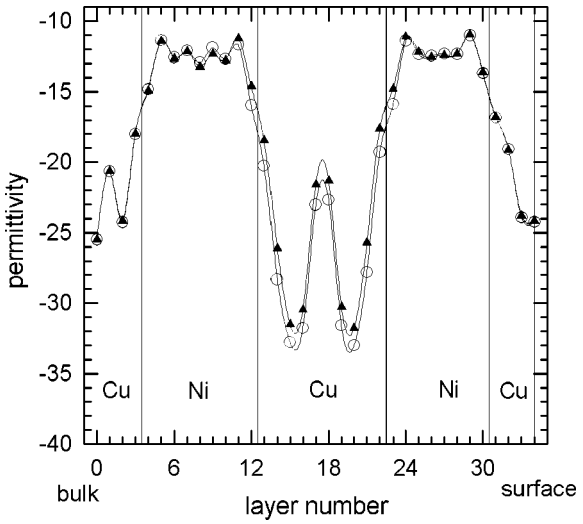

FIG. 4. Comparison of the AFM (triangles) and FM (circles) layer-resolved complex permittivity $\mathrm{Re}(\varepsilon_{xx})$ for $Cu_4Ni_8Cu_{10}Ni_9/Cu(100)$.

ellipticities in terms of the 2×2 matrix technique.[4] This implies that ε^p_{xy} is the only quantity in the description of MOKE that appears with an opposite sign in an AFM as compared to a FM configuration.

Neglecting multiple reflections and interferences, it is simple to analyze an incident wave reflected at a particular layer p. Assuming no further reflections, the light travels back to the surface with a reduced amplitude A'. The space like part of a plane wave traveling in the z direction is given by $A\exp(ikz)$. The wave number k is complex; thus, the real part is responsible for the oscillation and the imaginary part for the absorption of the wave. Using layer-resolved complex wave numbers the damped amplitude A'_p can be obtained as

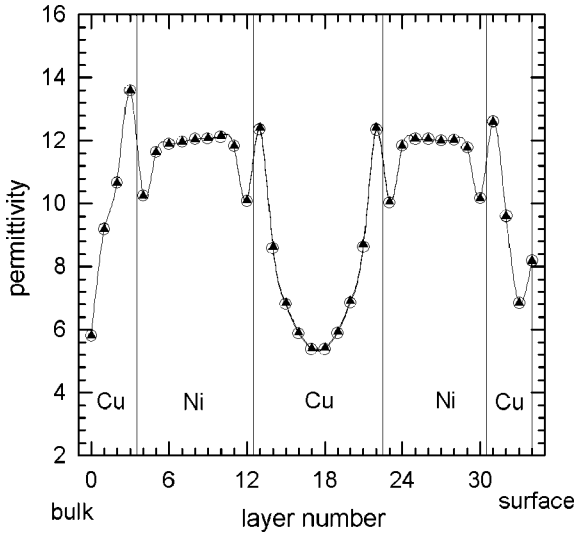

FIG. 5. Comparison of the AFM (triangles) and FM (circles) layer-resolved complex permittivity $\mathrm{Im}(\varepsilon_{xx})$ for $Cu_4Ni_8Cu_{10}Ni_9/Cu(100)$.

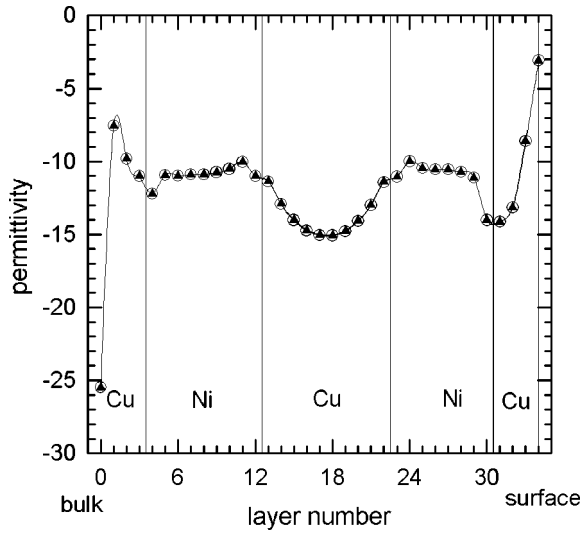

FIG. 6. Comparison of the AFM (triangles) and FM (circles) layer-resolved complex permittivity $\mathrm{Re}(\varepsilon_{zz})$ for $Cu_4Ni_8Cu_{10}Ni_9/Cu(100)$.

$$A'_p = A_0 \prod_{q=0}^{N-p+1} \prod_{q=N-p+1}^{0} \exp[i\ \mathrm{Im}(k_{N-q})d_{N-q}]$$
$$= A_0 \prod_{q=0}^{N-p+1} \exp[2i\ \mathrm{Im}(k_{N-q})d_{N-q}]. \quad (2)$$

If the penetration depth is defined as the thickness at which the amplitude of the incident wave is reduced to A_0/e, where e is Euler's constant, the number of layers, s, needed for this purpose has to be determined from

$$\sum_{q=0\in\{1,\ldots,s\}} \mathrm{Im}(k_{N-q})d_{N-q} = -1. \quad (3)$$

It should be noted that for the penetration depth only light traveling in the direction of the substrate is considered; therefore, in Eq. (3) the factor 2 is dropped. The bulk value of the refractive index of pure Cu, e.g., leads to a penetration depth of $s=68.5$ layers.

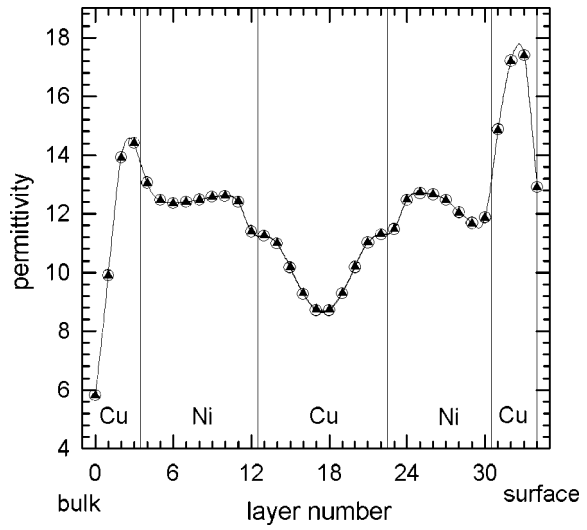

FIG. 7. Comparison of the AFM (triangles) and FM (circles) layer-resolved complex permittivity $\mathrm{Im}(\varepsilon_{zz})$ for $Cu_4Ni_8Cu_{10}Ni_9/Cu(100)$.

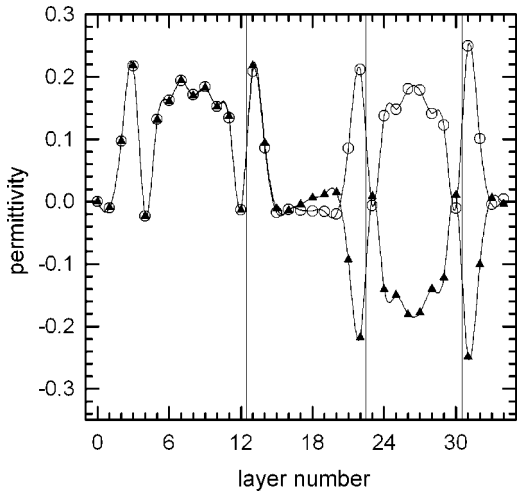

FIG. 8. Comparison of the AFM (triangles) and FM (circles) layer-resolved complex permittivity $\mathrm{Re}(\varepsilon_{xy})$ for $Cu_4Ni_8Cu_{10}Ni_9/Cu(100)$.

Assuming that MOKE is related to a weighted sum of the layer-resolved magnetic moments with weighting factors being the damping factors of a wave reflected at a layer p, the total damped magnetic moment is given by

$$m' = \sum_{p=1}^{N} m'_p, \quad m'_p = \frac{A'_p}{A_0} m_p. \quad (4)$$

The total damped magnetic moment m' (see Fig. 10) turns out to be negative for an AFM configuration which, as summarized in Table II, is then consistent with the theoretical MOKE results obtained using the 2×2 matrix technique.[4] In Fig. 11 m_p and m'_p in $Cu_4Ni_8Cu_nNi_9/Cu(100)$ are shown as a

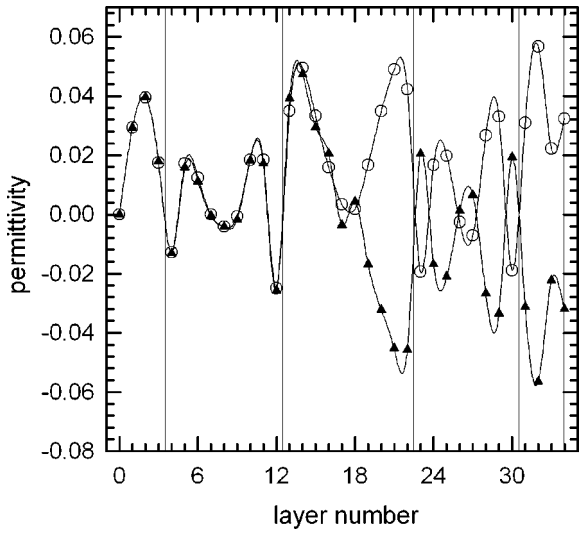

FIG. 9. Comparison of the AFM (triangles) and FM (circles) layer-resolved complex permittivity $\mathrm{Im}(\varepsilon_{xy})$ for $Cu_4Ni_8Cu_{10}Ni_9/Cu(100)$.

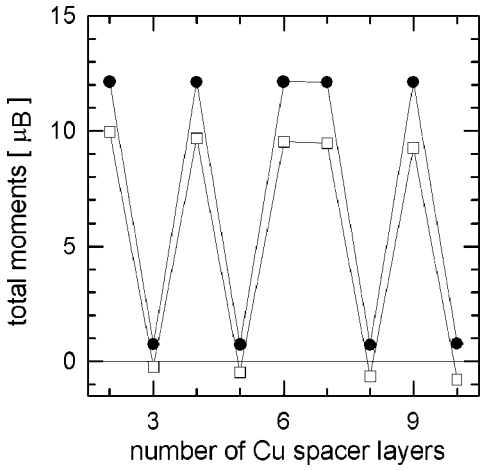

FIG. 10. Damped (squares) and undamped (circles) total magnetic moments in $Cu_4Ni_8Cu_{10}Ni_9/Cu(100)$ versus the number of Cu spacer layers.

function of the layer index p. In this figure, in which the Cu substrate is to the left, vacuum to the right, and the damping factor is displayed in terms of circles, one can see that especially in the Ni slab closer to the substrate the damped magnetic moments are considerably smaller than the undamped ones.

It should be noted that empirical information depth profiles were already introduced[6,7] in the early 1990s by defining so-called sensitivity functions. Thus it appears at a first glance that in Eq. (4) only a well-known recipe is applied. This, however, is not quite the case, since the layer-resolved magnetic moments m_p in this equation are calculated by means of an *ab initio* approach and the amplitudes A_p' simply mimic a (possible) exponential decay. The weights A_p'/A_0 are only introduced in order to show that in Kerr measurements not the true total magnetic moment is mapped but a quantity that reflects a perhaps rather complicated thickness dependence.

IV. SUMMARY

It was shown that the *ab initio*–calculated polar magneto-optic Kerr effect can be used to determine unambiguously the magnetic configuration (AFM or FM) in magnetic multilayer systems. The variation of Kerr rotation and ellipticity angles with respect to the number of spacer layers follows very closely previous experimental and theoretical investigations of the interlayer exchange coupling for the system,[1] $Cu_4Ni_8Cu_nNi_9/Cu(100)$, $n=2,\ldots,10$. It also turned out that the commonly accepted *direct* relationship between the total magnetic moment and MOKE has to be modified by taking a finite penetration depth into account. In order to show this a simple model for the depth dependence of the layer-resolved magnetic moments was used such that no additional empirical parameters had to be assumed. In particular it was shown that optically the main difference between a ferromagnetic and an antiferromagnetic configuration is manifested essentially in the off-diagonal elements of the layer-resolved permittivity tensor.

TABLE II. Comparison of theoretical MOKE results as given by θ_K and ϵ_K with damped (m') and undamped (m) total magnetic moments.

	FM	AFM
θ_K, ϵ_K	>0	<0
m'	>0	<0
m	>0	>0

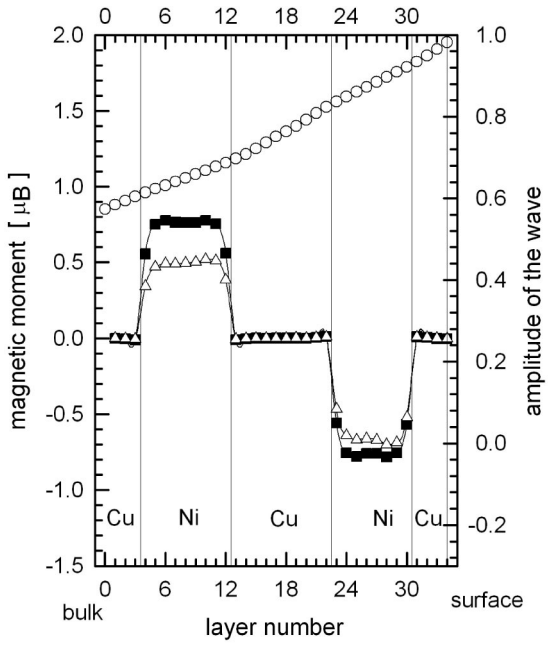

FIG. 11. Layer-resolved plane-wave amplitudes A_p' (circles) in $Cu_4Ni_8Cu_{10}Ni_9/Cu(100)$, assuming that the initial amplitude A_0 is unity. Squares and triangles refer in turn to layer-resolved undamped and damped magnetic moments.

ACKNOWLEDGMENTS

Financial support from the Austrian Science Foundation (Project No. W004), Austrian Ministries (Grant Nos. GZ 45.531, Zl 98.366) Wissenschaftlich–Technisches Abkommen Austria-Hungary (A-3/03), and Hungarian National Science Foundation (OTKA Grant Nos. T037856, T046267) is gratefully acknowledged. We also wish to thank the computing center IDRIS at Orsay as most of the calculations were performed using their facilities.

[1] R. Hammerling, J. Zabloudil, P. Weinberger, J. Lindner, E. Kosubek, R. Nünthel, and K. Baberschke, Phys. Rev. B **68**, 092406 (2003).

[2] L. Szunyogh, B. Újfalussy, P. Weinberger, and J. Kollár, Phys. Rev. B **49**, 2721 (1994); L. Szunyogh, B. Újfalussy, and P. Weinberger, *ibid.* **51**, 9552 (1995). For a detailed description see also J. Zabloudil, R. Hammerling, L. Szunyogh, and P. Weinberger, *Electron Scattering in Solid Matters: A Theoretical and Computational Treatise* (Springer-Verlag, Heidelberg, in press).

[3] L. Szunyogh and P. Weinberger, J. Phys.: Condens. Matter **11**, 10451 (1999); A. Vernes, L. Szunyogh, and P. Weinberger, Phase Transitions **75**, 167 (2002).

[4] A. Vernes, L. Szunyogh, and P. Weinberger, Phys. Rev. B **65**, 144448 (2002); **66**, 214404 (2002); I. Reichl, A. Vernes, L. Szunyogh, C. Sommers, P. Mohn, and P. Weinberger, Philos. Mag. B **84**, 2543 (2004).

[5] P. N. Argyres, Phys. Rev. **97**, 334 (1955).

[6] G. Traeger, L. Wenzel, and A. Hubert, Phys. Status Solidi A **131**, 201 (1992).

[7] A. Hubert and G. Traeger, J. Magn. Magn. Mater. **124**, 185 (1993).